Journal of
Synchrotron
Radiation

ISSN 1600-5775

Received 27 September 2013
Accepted 2 December 2013

Local structure of amorphous tellurium studied by EXAFS

Hiroyuki Ikemoto[a]* and Takafumi Miyanaga[b]

[a]Department of Physics, University of Toyama, Toyama 930-8555, Japan, and [b]Department of Advanced Physics, Hirosaki University, Hirosaki 036-8561, Japan.
*E-mail: ikemoto@sci.u-toyama.ac.jp

The local structure of an amorphous tellurium (a-Te) film was investigated by extended X-ray absorption fine-structure analysis. The covalent bond length shortens and the Debye–Waller factor of the intra-chain decreases in a-Te compared with trigonal Te (t-Te). The value of the intra-chain coordination number is close to two, which is the value for t-Te, and the inter-chain interaction weakens. These results suggest that the primary chain structure remains intact, but the secondary structure is disrupted. The decrease in the inter-chain interaction strengthens the intra-chain interaction.

Keywords: amorphous tellurium; intra- and inter-chain interactions; local structure; EXAFS.

1. Introduction

Tellurium and selenium are unique elements that are characterized by hierarchical structures. In trigonal Te (t-Te) and Se (t-Se) the primary structure comprises infinite length chains consisting of covalently bonded atoms. In t-Te, the intra-chain first-nearest-neighbor (1NN) distance ($r_{\rm intra}$) is 2.835 Å and the inter-chain 1NN distance ($r_{\rm inter}$) is 3.495 Å (Adenis *et al.*, 1989). $r_{\rm inter}$ is smaller than twice the van der Waals radii (Batsanov, 2001), implying that the chains interact *via* stronger forces than the van der Waals forces. The chains are bound by overlapping electronic orbitals between the lone-pair and anti-bonding orbitals on adjacent chains. Such overlap brings about the elongation of the covalent bond. The piling of stacks of chains in the primary structure creates a secondary structure, which then affects the primary structure.

It is interesting to know the structure of amorphous tellurium (a-Te) and selenium (a-Se) considering the differences in the strength of their intra- and inter-chain interactions. It is better to study a-Te because there are clear peaks originating from the intra- and inter-chain first-neighbor correlations in the Fourier transform (FT) of the extended X-ray absorption fine-structure (EXAFS) functions. Many studies have been published for a-Se (Hohl & Jones, 1991; Kolobov *et al.*, 1997; Zhao & Rowlands, 1995) but only a few for a-Te. a-Se can be easily created by the solidification of liquid Se or by the deposition of Se. In contrast to a-Se, a-Te is prepared *via* condensation on substrate at liquid-helium or liquid-nitrogen (LN_2) temperatures. The structure of thin tellurium films deposited at LN_2 temperature was investigated by electron diffraction (Ichikawa, 1973; Kohzu & Taketoshi, 2002). These studies revealed that the films are amorphous, and the atoms in a-Te are arranged in short chains with many threefold-coordinated atoms. NMR (Koma *et al.*, 1971) and Raman spectroscopy (Brodsky *et al.*, 1972) also suggest the existence of chains. According to NMR-based estimates, a chain may contain about ten Te atoms; on the other hand, the Raman spectrum of a-Te may show longer chains.

We have investigated the local structure of the tellurium nanoparticles (n-Te) by EXAFS and X-ray diffraction (XRD) (Ikemoto & Miyanaga, 2007; Ikemoto *et al.*, 2011). The fraction of the amorphous-like phase increases as the size of n-Te decreases. The primary structure is preserved, whereas the secondary structure is disrupted. Information on the local structure of a-Te is useful for understanding that of n-Te.

We present the local structure of a-Te based on the EXAFS results, and we focus on the relation between the intra- and inter-chain interactions.

2. Experimental

Prior to the deposition of Te, NaCl (99.99% purity) was deposited from an alumina crucible on a carbon sheet at room temperature. Te (99.999% purity) was deposited onto the substrates from a crucible. The thickness of the Te film was 300 nm, which was monitored with a quartz oscillator sensor (ULVAC CRTS-4) and a deposition controller (ULVAC CRTM6000). We performed EXAFS measurements for two types of Te films: the first was deposited on a substrate maintained at room temperature, whereas the second was deposited on a substrate maintained at LN_2 temperature. As mentioned above, the Te film deposited at room temperature is trigonal, whereas that deposited at LN_2 temperature is amorphous. We named the former t-Te and the latter a-Te.

X-ray absorption measurements were performed using the spectrometer installed at NW10A of the Photon Factory (PF-AR) in the High Energy Accelerator Research Organization (KEK), Tsukuba, Japan. EXAFS data were obtained in

fluorescence mode for the Te *K*-edge (31.8 keV). The intensity of the incident beam (I_0) was monitored using an ionization chamber filled with Ar gas, and X-ray fluorescence was monitored using a multi-element solid-state Ge detector. EXAFS measurements were performed at LN_2 temperature. The a-Te sample was maintained at LN_2 temperature throughout sample preparation and EXAFS measurements. The EXAFS data were analyzed using the *miXAFS* code (Ikemoto *et al.*, 2011). Phase shift, backscattering amplitude and electron mean free path were calculated using the *FEFF8* code (Ankudinov *et al.*, 1998).

3. Results

Fig. 1 shows the EXAFS oscillations $k^2\chi(k)$ of a-Te and t-Te as a function of the photoelectron wavenumber k. Distinct EXAFS oscillations are observed up to 16.0 Å^{-1}. The amplitudes for a-Te and t-Te are similar, but the period of oscillation for a-Te is slightly longer than that for t-Te.

The FT of the $k\chi(k)$ data provides useful information for identifying atomic correlations. $k\chi(k)$ was Fourier transformed in the k-range from 2.0 to 16.0 Å^{-1}, where a Hamming window was used to reduce the ripples in the FT in r-space. Fig. 2 shows the FT of $k\chi(k)$ for a-Te and t-Te as a function of the radial distance. There are three prominent peaks at 2.88, 3.54 and 4.53 Å in the FT of t-Te. By comparing these with XRD data in the literature (Adenis *et al.*, 1989), we can assign the first and second peaks to contributions from the intra- and inter-chain 1NN correlations, respectively. The third peak corresponds to the second-nearest-neighbor distances of the intra- and inter-chain correlations, which are 4.441 and 4.456 Å, respectively. The shoulder at 5.1 Å corresponds to the third-nearest-neighbor distance of the intra-chain.

The first and second peaks are present even in the FT of a-Te. The intensity of the first peak of the FT for a-Te is comparable with that for t-Te; however, the decrease in the higher-order peaks for a-Te is larger than in t-Te. The peak position of the intra-chain 1NN for a-Te is clearly shorter than that for t-Te. This suggests that, in a-Te, the chain structures are preserved, but the inter-chain interactions weaken.

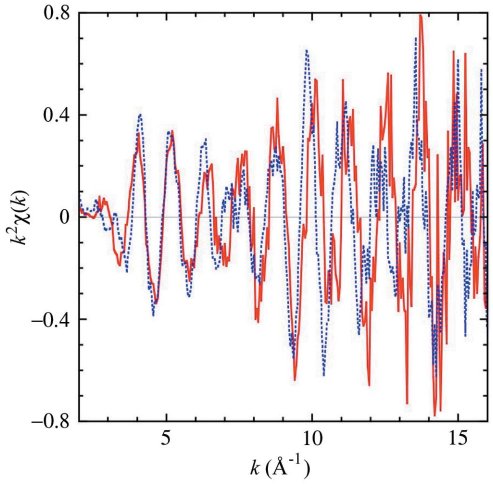

Figure 1
EXAFS spectra $k^2\chi(k)$ for t-Te (blue dotted line) and a-Te (red solid line).

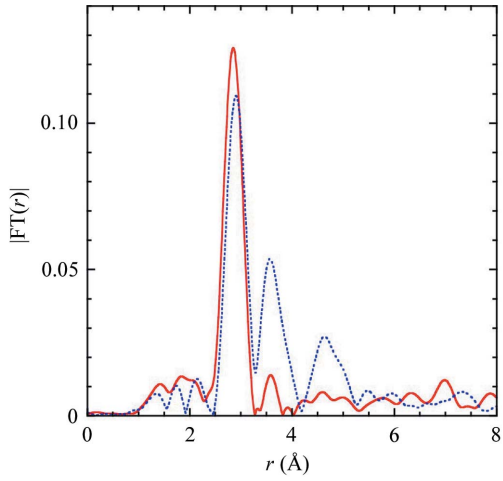

Figure 2
Fourier transform magnitude of the EXAFS $k\chi(k)$ data for t-Te (blue dotted line) and a-Te (red solid line).

In the region above 4 Å there are many peaks; therefore, they cannot be assigned to atomic correlations. In amorphous materials, structural flexibility increases with higher-order correlations. The distribution of the intra-chain second-nearest-neighbor atomic distance may be widespread, causing the disappearance of the peak. Similar phenomena are also observed in the case of amorphous Ge (Dalba *et al.*, 1995).

To extract the peaks originating from the intra- and inter-chain 1NNs, the FT peaks were Fourier-filtered in the range 2.38–3.82 Å and 2.46–4.18 Å for a-Te and t-Te, respectively. To study the intra- and inter-chain 1NNs, least-squares fitting was applied to the Fourier-filtered $k^2\chi(k)$. The free parameters were the atomic distance (r), the coordination number (N), the Debye–Waller factor (DW) and the third cumulant (C_3) for the intra- and inter-chain 1NN correlations. The energy shift was determined to minimize the R-factor for t-Te. The scaling factor was adjusted to 2, according to the value of the intra-chain 1NN coordination number ($N_{\rm intra}$) for t-Te.

In the EXAFS analysis the structural parameters correlate with each other, and there is an especially strong correlation between N and DW. To check this correlation, we performed least-squares fitting with fixed $N_{\rm inter}$ and $DW_{\rm inter}$. Fig. 3 shows the three-dimensional shaded surface plot for t-Te, which is one function of the *miXAFS* code (Ikemoto *et al.*, 2011). The x-, y- and z-axis represent $N_{\rm inter}$, $DW_{\rm inter}$ and R-factor, respectively. There is only one clear deep trough, which can be used to determine the values of $N_{\rm inter}$ and $DW_{\rm inter}$ at the trough.

Fig. 4 shows the calculated surface plot for a-Te. The surface is mostly flat with a very shallow valley as compared with t-Te. The instability of the least-squares fitting suggests that the contribution from the inter-chain is probably small. Hence, we do not discuss the inter-chain, and we focus on the intra-chain structural parameters. To extract only the intra-chain 1NN peak, the FT peak was filtered in the range 2.45–3.30 Å for

Table 1
Structural parameters obtained from the fit to the experimental EXAFS spectra for a-Te and t-Te.

The values obtained by X-ray (Adenis *et al.*, 1989) and electron (Ichikawa, 1973) diffraction are also shown.

	r_{intra} (Å)	N_{intra}	DW_{intra} (Å)	$C_{3,\ intra}$ $\times 10^{-4}$ (Å^3)	*R*-factor (Ikemoto *et al.*, 2011)
t-Te (Adenis *et al.*, 1989)	2.835	2.00			
t-Te	2.83 ± 0.02	2.00	0.054 ± 0.002	0.1 ± 1.9	12.9
a-Te	2.77 ± 0.02	1.97 ± 0.20	0.049 ± 0.002	−1.6 ± 1.9	16.6
a-Te (Ichikawa, 1973)	2.79 ± 0.01	1.8			

a-Te. The Fourier-filtered $\chi(k)$ for a-Te was analyzed with a one-site model. The values of r_{intra} and N_{intra} are shown in Table 1, which lists the structural parameters from X-ray diffraction measurements at room temperature (Adenis *et al.*, 1989). The r_{intra} values of this study for t-Te do not deviate from the literature values.

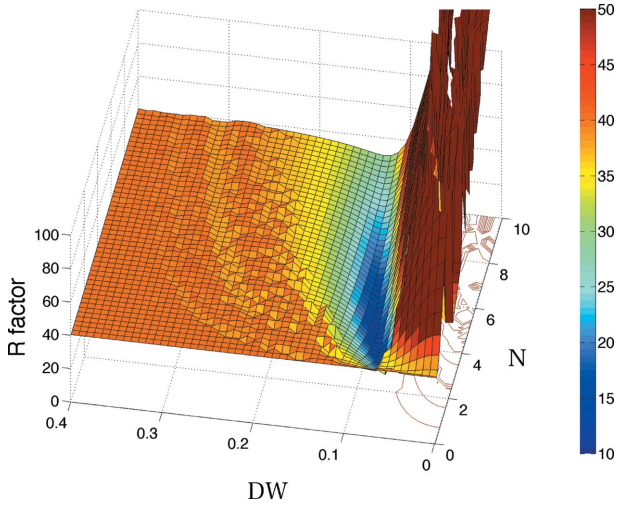

Figure 3
Three-dimensional shaded surface plot for t-Te. The *x*-, *y*- and *z*-axis represent N_{inter}, DW_{inter} and *R*-factor, respectively. The color and surface height are proportional to the *R*-factor.

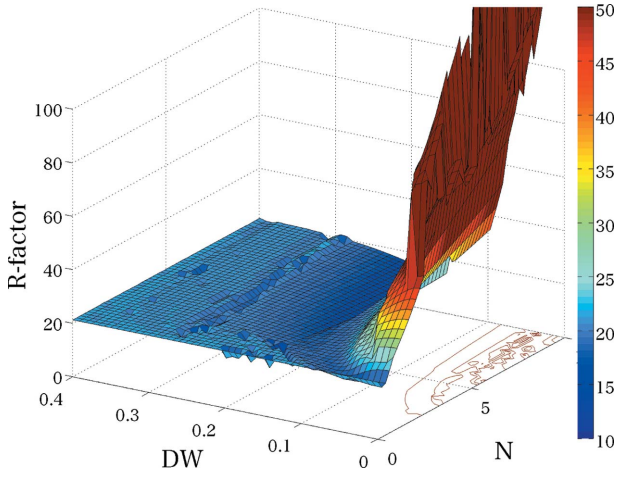

Figure 4
Three-dimensional shaded surface plot for a-Te. The *x*-, *y*- and *z*-axis represent N_{inter}, DW_{inter} and *R*-factor, respectively. The color and surface height are proportional to the *R*-factor.

As seen in Table 1, r_{intra} for a-Te is shorter than for t-Te in 0.06 Å. N_{intra} for a-Te is very close to 2, which is the value for the coordination number of t-Te. *DW* for a-Te is smaller than that for t-Te by 10%. The value of C_3 is almost zero within error; thus, no significant difference is seen between t-Te and a-Te.

4. Discussion

The structure of a-Te has been experimentally investigated by electron diffraction (Ichikawa, 1973; Kohzu & Taketoshi, 2002) and *ab initio* methods (Akola & Jones, 2012). These studies portray a-Te as having short chains with onefold-coordinated and threefold-coordinated Te atoms in addition to the normal twofold-coordinated atoms.

This study is the first EXAFS report for a-Te. The intra-chain 1NN atomic distance is 2.77 Å, which is 0.06 Å shorter than that for t-Te. As argued for Te nanoparticles, the covalent bond length reflects the strength of the shorter bond (Ikemoto *et al.*, 2011). The small *DW* value means small fluctuations of atoms. The small values of the covalent bond length and *DW* mean that the covalent bond strengthens in a-Te.

The EXAFS experiments have the advantage of investigating the local structure, whereas diffraction methods (electron, X-ray and neutron diffractions) are better for studying the medium- and long-range order. EXAFS spectroscopy gives structural information up to 6 Å, whereas diffraction methods have a wider range. EXAFS spectroscopy can be used to study the structure of nanoparticles and disordered materials. The advantages of EXAFS spectroscopy are due to the local interferences among the photoelectrons emitted from the X-ray absorbing atoms and scattered from the surrounding atoms. Thus, differences appear in the FT of the EXAFS functions and the structure factors of electron diffraction. In Fig. 2 the second peak originating from the inter-chain 1NN is well separated, whereas that arising from electron diffraction overlaps with other peaks.

Because the error of the coordination number is 5–10% in the EXAFS analysis, the intra-chain 1NN coordination number for a-Te is 1.97 ± 0.20, which is the same as that for t-Te within experimental error. This is consistent with Raman data (Brodsky *et al.*, 1972). As mentioned above, N_{intra} is 2.00 within error; on the other hand, electron diffraction (Ichikawa, 1973) and NMR (Koma *et al.*, 1971) studies gave a lower value, suggesting that a-Te consists of short chains. It is difficult to judge which value is correct; thus, we consider that N_{intra} = 2.

One reason is the advantage of EXAFS in the short-range order. The second is the uncertainty of N_{intra} in the radial distribution function of the diffraction measurements. As pointed out by Akola & Jones (2012), the coordination number has a certain level of uncertainty depending on the integrated region. If the covalent bonds could be judged on the basis of electron density, such differences could be resolved. The calculated N_{intra} confirms the assumptions of the a-Se-Te EXAFS analysis (Majid *et al.*, 1998).

We show that the twofold chain structure is maintained in a-Te, but the inter-chain interactions decrease. Thus, the overlap between the lone-pair and the anti-bonding orbitals in adjacent chains decreases, which shortens the covalent bond length.

5. Conclusion

We prepared a-Te film at LN_2 temperature and immediately measured its EXAFS spectra while maintaining the temperature. The covalent bond length shortens by 0.06 Å compared with t-Te; nonetheless, the coordination number is similar to that for t-Te. The inter-chain interaction weakens, which strengthens the intra-chain interaction as observed in Te nanoparticles.

The authors thank Mr M. Fujita, T. Watanabe, A. Oono and Ms M. Seo for their assistance at various stages of this study. This work was supported by JSPS KAKENHI grant No. 23510120 and the Kurata Memorial Hitachi Science and Technology Foundation. The synchrotron radiation experiments were performed at the Photon Factory in KEK under proposal No. 2011G579.

References

Adenis, C., Langer, V. & Lindqvist, O. (1989). *Acta Cryst.* C**45**, 941–942.
Akola, J. & Jones, R. O. (2012). *Phys. Rev. B*, **85**, 134103.
Ankudinov, A. L., Ravel, B., Rehr, J. J. & Conradson, S. D. (1998). *Phys. Rev. B*, **58**, 7565–7576.
Batsanov, S. S. (2001). *Inorg. Mater.* **37**, 871–885.
Brodsky, M. H., Gambino, R. J., Smith, J. E. Jr & Yacoby, Y. (1972). *Phys. Status Solidi B*, **52**, 609–614.
Dalba, G., Fornasini, P. & Grazioli, M. (1995). *Phys. Rev. B*, **52**, 11034–11043.
Hohl, D. & Jones, R. O. (1991). *Phys. Rev. B*, **43**, 3856–3870.
Ichikawa, T. (1973). *Phys. Status Solidi B*, **56**, 707–715.
Ikemoto, H., Goyo, A. & Miyanaga, T. (2011). *J. Phys. Chem. C*, **115**, 2931–2937.
Ikemoto, H. & Miyanaga, T. (2007). *Phys. Rev. Lett.* **99**, 165503.
Kohzu, K. & Taketoshi, K. (2002). *Jpn. J. Appl. Phys.* **41**, 6084–6088.
Kolobov, A. V., Oyanagi, H., Tanaka, K. & Tanaka, K. (1997). *Phys. Rev. B*, **55**, 726–734.
Koma, A., Mizuno, O. & Tanaka, S. (1971). *Phys. Status Solidi B*, **46**, 225–233.
Majid, M., Benazeth, S., Souleau, C. & Purans, J. (1998). *Phys. Rev. B*, **58**, 6104–6114.
Zhao, W. & Rowlands, J. A. (1995). *Med. Phys.* **22**, 1595–1604.